A hyperluminous obscured quasar at a redshift of z ≈ 4.3

Andreas Efstathiou, Katarzyna Malek, Denis Burgarella, Peter Hurley, Seb Oliver, Veronique Buat, Raphael Shirley, Steven Duivenvoorden, Vicky Papadopoulou Lesta, Duncan Farrah, et al.

Monthly Notices of the ROYAL ASTRONOMICAL SOCIETY
MNRAS **503,** L11–L16 (2021) doi:10.1093/mnrasl/slaa206

A hyperluminous obscured quasar at a redshift of $z \approx 4.3$

Andreas Efstathiou,[1]★ Katarzyna Małek,[2,3] Denis Burgarella,[3] Peter Hurley,[4] Seb Oliver,[4] Veronique Buat,[3] Raphael Shirley,[4,5,6] Steven Duivenvoorden,[4] Vicky Papadopoulou Lesta,[1] Duncan Farrah,[7,8] Kenneth J. Duncan[9,10] and María del Carmen Campos Varillas[4]

[1]*School of Sciences, European University Cyprus, Diogenes Street, Engomi, 1516 Nicosia, Cyprus*
[2]*National Centre for Nuclear Research, ul. Pasteura 7, 02-093 Warszawa, Poland*
[3]*Aix Marseille Univ., CNRS, CNES, LAM Marseille, France*
[4]*Astronomy Centre, Department of Physics and Astronomy, University of Sussex, Brighton BN1 9QH, UK*
[5]*Instituto de Astrofísica de Canarias, E-38205 La Laguna, Tenerife, Spain*
[6]*Universidad de La Laguna, Dpto. Astrofísica, E-38206 La Laguna, Tenerife, Spain*
[7]*Department of Physics and Astronomy, University of Hawaii, 2505 Correa Road, Honolulu, HI 96822, USA*
[8]*Institute for Astronomy, 2680 Woodlawn Drive, University of Hawaii, Honolulu, HI 96822, USA*
[9]*Royal Observatory Edinburgh, University of Edinburgh, Blackford Hill, Edinburgh EH9 3HJ, UK*
[10]*Sterrewacht Leiden, Universiteit Leiden, Leiden, the Netherlands*

Accepted 2020 December 21. Received 2020 December 21; in original form 2020 July 14

ABSTRACT

In this work we report the discovery of the hyperluminous galaxy HELP_J100156.75 + 022344.7 at a photometric redshift of $z \approx 4.3$. The galaxy was discovered in the Cosmological Evolution Survey (COSMOS) field, one of the fields studied by the *Herschel* Extragalactic Legacy Project (HELP). We present the spectral energy distribution (SED) of the galaxy and fit it with the CYprus models for Galaxies and their NUclear Spectra (CYGNUS) multi-component radiative transfer models. We find that its emission is dominated by an obscured quasar with a predicted total 1–1000 μm luminosity of $3.91^{+1.69}_{-0.55} \times 10^{13}\,L_{\odot}$ and an active galactic nucleus (AGN) fraction of ~ 89 per cent. We also fit HELP_J100156.75 + 022344.7 with the CIGALE(CODE INVESTIGATING GALAXY EMISSION) code and find a similar result. This is only the second $z > 4$ hyperluminous obscured quasar discovered to date. The discovery of HELP_J100156.75 + 022344.7 in the $\sim$2 deg^2 COSMOS field implies that a large number of obscured hyperluminous quasars may lie in the HELP fields, which cover $\sim$1300 deg^2. If this is confirmed, tension between supermassive black hole evolution models and observations will be alleviated. We estimate the space density of objects like HELP_J100156.75 + 022344.7 at $z \approx 4.5$ to be $\sim 1.8 \times 10^{-8}$ Mpc^{-3}. This is slightly higher than the space density of coeval hyperluminous optically selected quasars, suggesting that the obscuring torus in $z > 4$ quasars may have a covering factor $\gtrsim 50$ per cent.

Key words: galaxies: active – galaxies: formation – galaxies: high-redshift – infrared: galaxies – submillimetre: galaxies.

1 INTRODUCTION

Ever since the discovery of quasars in the 1960s, numerous surveys searching for quasars of ever-increasing redshift have been carried out. The main motivation of the surveys was to take advantage of the extreme luminosity of quasars to search for distant objects that probe the conditions in the early history of the Universe. Luminous quasars selected at optical and near-infrared wavelengths have now been observed out to $z > 6$ (e.g. Wu et al. 2015), corresponding to an epoch less than a billion years after the big bang. Currently, just a handful of quasars have also been discovered at $z > 7$ (e.g. Mortlock et al. 2011; Banados et al. 2018; Wang et al. 2018; Yang et al. 2020).

The observed space density of quasars rises steeply from $z \sim$ 6–7, reaching a peak at $z \sim 2$ (e.g. Kelly et al. 2010), and then declines again towards $z \sim 0$. In the redshift range 0–3, the black hole accretion rate density (BHAD) and the star formation rate density (SFRD) correlate (e.g. Delvecchio et al. 2014) and this is one of the reasons why accretion of matter on to supermassive black holes (SMBH) in quasars, or more generally active galactic nuclei (AGNs), and star formation are believed to be interrelated phenomena (e.g. Fabian 2012; Hickox & Alexander 2018). At $z > 3$, however, a large deviation between SFRD and BHAD is observed, with BHAD being much lower than predicted by SMBH evolution models (Vito et al. 2018).

The deviation between BHAD and SFRD may be due to the fact that there are large numbers of obscured quasars at $z > 3$ that have not yet been discovered. This is expected from the unified model for AGNs (Antonucci 1993) if it holds at high redshift. The model postulates the existence of a geometrically and optically thick dusty torus, an idea that is well tested in the local Universe, which obscures the central engine and reprocesses its optical and ultraviolet radiation to predominantly 3–30 μm radiation. However, the mean covering factor of the torus, which determines the proportion of quasars that

★ E-mail: A.Efstathiou@euc.ac.cy

are obscured, may depend on redshift as well as luminosity (e.g. Hickox & Alexander 2018). Detecting obscured AGNs at $z > 3$ is made difficult by the fact that the peak of the emission from the torus shifts to the far-infrared. X-ray telescopes also currently lack the sensitivity to find obscured AGNs at $z > 3$ unless they are extremely luminous.

The *Wide-field Infrared Survey Explorer* (*WISE*) carried out a survey of the whole sky at mid-infrared wavelengths and detected a large number of objects that are especially luminous at those wavelengths (Eisenhardt et al. 2012, Bridge et al. 2013). These objects have been named Hot Dust Obscured Galaxies (Hot DOGs) and are believed to be powered by emission by an obscured AGN (e.g. Jones et al. 2015; Farrah et al. 2017). However, to date only one $z > 4$ obscured AGN has been found by *WISE*, the extremely luminous infrared galaxy W2246−0526 at $z = 4.6$ with a luminosity of $\sim 3 \times 10^{14}\,L_{\odot}$ (Tsai et al. 2015, 2018), making it the most luminous galaxy observed to date. Diaz-Santos et al. (2018) recently imaged W2246−0526 with the Atacama Large Millimeter/submillimeter Array (ALMA) and found it to be a multiple merger.

The *Herschel* Extragalactic Legacy Project (HELP: Shirley et al. 2019; Shirley et al., in preparation), which assembled ultraviolet to submillimetre spectral energy distributions for over 170 million galaxies in about 1300 deg^2 of the sky, is much deeper than *WISE*. Early results from HELP have been presented in Małek et al. (2018). The HELP database, which is already public, is therefore much more suitable for determining the space density of $z > 4$ obscured quasars and exploring the physics of AGNs and their role in galaxy evolution at those redshifts.

In this work, we report the discovery of an obscured AGN in the Cosmological Evolution Survey (COSMOS) field (Scoville et al. 2007) with an estimated photometric redshift of 4.48 (Laigle et al. 2016), which was discovered as part of the HELP project. The catalogue name of the source is HELP_J100156.758+022344.739, but in the remainder of this work we will refer to it as HELP_J100156.75+022344.7. We use the CYprus models for Galaxies and their NUclear Spectra (CYGNUS) multi-component radiative transfer models for AGN tori, starbursts, and spheroidal hosts to fit the spectral energy distribution (SED) of HELP_J100156.75 + 022344.7 with the MCMC code SATMC (Johnson et al. 2013). Using SATMC, we also simultaneously obtain a photometric redshift using all of the multiwavelength data used in the SED fit. For comparison, we also fit the SED of HELP_J100156.75 + 022344.7 with the CIGALE code (Noll et al. 2009; Boquien et al. 2019) and find similar results.

In Section 2 of this work, we discuss the method of assembling the multiwavelength observations, in Section 3 we discuss the radiative transfer models we used and the method of fitting the SED of HELP_J100156.75 + 022344.7, and in Section 4 we discuss our results. We assume a standard cosmology with $H_0 = 70$ km s^{-1} Mpc^{-1}, $\Omega = 1$, and $\Lambda = 0.7$.

2 OBSERVATIONS

HELP uses prior information from optical, near-infrared, and mid-infrared surveys to deal with blending in the confusion-limited maps from the *Herschel Space Observatory* (Pilbratt et al. 2010). Hurley et al. (2017) developed the XID+ method of deblending confused *Herschel* sources. One of the first fields analysed with XID+ was the well-studied COSMOS field (Scoville et al. 2007), in which we identified HELP_J100156.75 + 022344.7. Shirley et al (2019) describe in detail the process of constructing the HELP catalogue from pristine catalogues produced by other independent teams. The HELP photometry for HELP_J100156.75+022344.7 that we use in the rest of this work, which is the result of the standard default processing by XID+, is listed in Table 1. The source is very faint in the optical and this partly explains why a spectrum is not available. For example, the *AB* magnitude in the SUPRIME RC filter is 26.2. The source is not detected in the Subaru *B* and *V* filters (Laigle et al. 2016). We use these data as upper limits in our analysis. The photometric uncertainties of the Spectral and Photometric Imaging Receiver (SPIRE) data points are relatively small, as HELP_J100156.75 + 022344.7 is fairly isolated in the SPIRE images. This is shown in Fig. 1, where all the detections are plotted, and in Fig. S4 in Appendix B, where the *p*-value maps derived by XID+ are plotted. We have checked whether HELP_J100156.75 + 022344.7 is included in the 70-μm catalogue of Frayer et al (2009). The nearest 70-μm source is 1.27 arcmin away from HELP_J100156.75+022344.7. We have used the noise of the Frayer et al. map at the approximate position of HELP_J100156.75 + 022344.7 to set an upper limit at 70 μm, which we use in the SED fit. HELP_J100156.75 + 022344.7 is detected in the Very Large Array (VLA)–COSMOS 3-GHz catalogue of Smolcic et al. (2017), who quote a flux of 27 ± 2.6 μJy and classify the source as a moderate-to-high radiative luminosity AGN. There are no detections in the *Chandra* catalogue of Marchesi et al. (2016) and the *X-ray Multi-Mirror* (*XMM*)–COSMOS catalogue of Cappelluti et al. (2009). The source is also very faint in the *Hubble Space Telescope* (*HST*) F814W image. In Fig. 1, we show postage stamps of the source in 18 different filters.

Table 1. Photometry for HELP_J100156.75 + 022344.7 from the optical to the submillimetre. The errors in the *Herschel* fluxes include the errors associated with the deblending.

Wavelength λ (μm)	Flux density S_ν (Jy)	Filter
0.446	$0.00 \pm 1.10 \times 10^{-8}$	Subaru $B^\dagger$
0.548	$0.00 \pm 2.10 \times 10^{-8}$	Subaru $V^\dagger$
0.628	$4.71 \pm 0.95 \times 10^{-8}$	MEGACAM R
0.650	$1.25 \pm 0.17 \times 10^{-7}$	SUPRIME RC
0.761	$1.21 \pm 0.13 \times 10^{-7}$	MEGACAM I
0.767	$1.57 \pm 0.24 \times 10^{-7}$	SUPRIME IP
0.873	$1.65 \pm 0.30 \times 10^{-7}$	SUPRIME Z
0.921	$5.31 \pm 0.65 \times 10^{-7}$	SUPRIME N921
1.645	$3.63 \pm 0.57 \times 10^{-7}$	VISTA H
2.147	$9.47 \pm 0.55 \times 10^{-7}$	VISTA Ks
3.54	$2.96 \pm 0.06 \times 10^{-6}$	IRAC 1
4.48	$2.39 \pm 0.05 \times 10^{-6}$	IRAC 2
5.7	$2.13 \pm 1.50 \times 10^{-6}$	IRAC $3^\dagger$
7.83	$9.63 \pm 2.27 \times 10^{-6}$	IRAC 4
24	$6.50 \pm 0.05 \times 10^{-4}$	MIPS24
70	$0.00 \pm 3.00 \times 10^{-3}$	MIPS70†
100	$5.15 \pm 1.12 \times 10^{-3}$	PACS
160	$1.01 \pm 1.00 \times 10^{-2}$	PACS†
250	$9.11 \pm 0.93 \times 10^{-3}$	SPIRE
350	$1.03 \pm 0.12 \times 10^{-2}$	SPIRE
500	$9.03 \pm 1.31 \times 10^{-3}$	SPIRE

Note. †Upper limit.

3 SED FITTING WITH THE CYGNUS RADIATIVE TRANSFER MODELS

In this section we describe the libraries of spheroidal galaxy, AGN torus, and starburst models used for the SED fitting of HELP_J100156.75 + 022344.7 with SATMC (Johnson et al. 2013). The models form part of the CYGNUS collection of radiative transfer

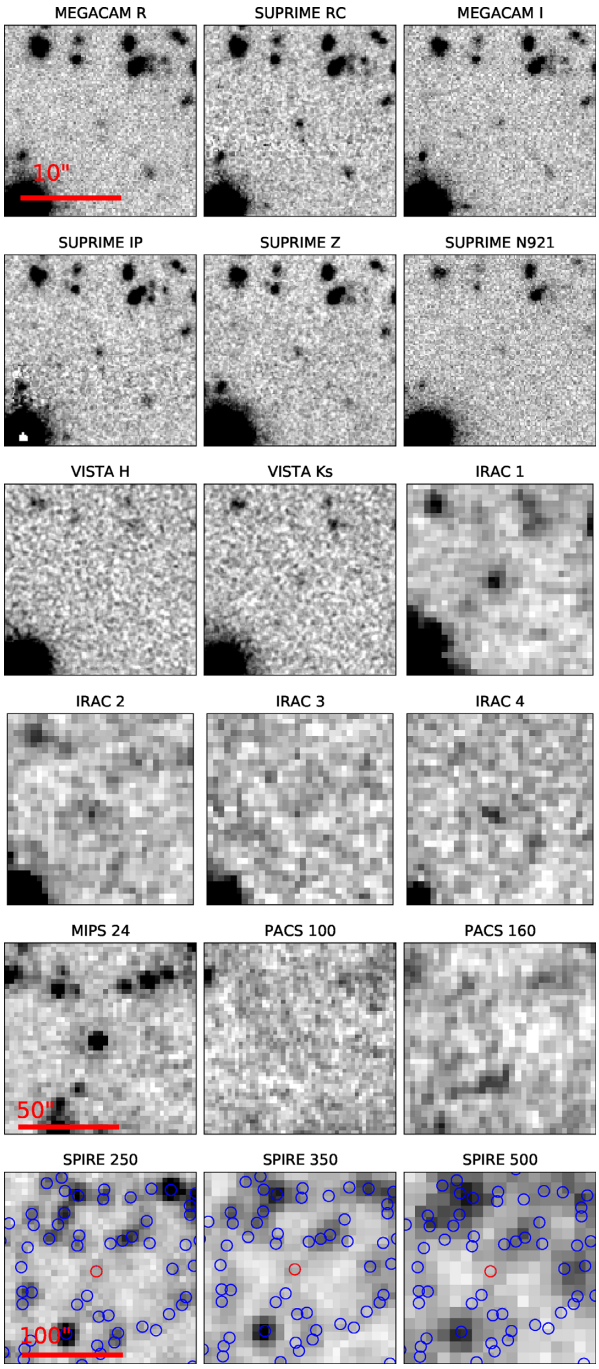

Figure 1. Postage stamps of HELP_J100156.75 + 022344.7 in all the filters listed in Table 1 and used in the SED fit, except MIPS70 and Subaru *B* and *V*, which are not included in HELP. In the last two rows we have zoomed out by factors of 5 and 10. The blue circles denote all detections by XID+ and the red circles the source.

models.[1] Various combinations of these models have been used extensively to interpret the observed SEDs of a broad range of galaxies, in e.g. Alexander et al. (1999), Ruiz et al. (2001), Farrah et al. (2002, 2003, 2012, 2017), Verma et al. (2002), Mattila et al. (2012, 2018), Efstathiou et al. (2013), Lonsdale et al. (2015), Harris et al. (2016), Herrero-Illana et al. (2017) and Pitchford et al. (2019).

[1]Available at http://ahpc.euc.ac.cy/

3.1 Spheroidal models

The method employed for computing the libraries of spheroidal models used in this work is an evolution of the cirrus model of Efstathiou & Rowan-Robinson (2003). As in Efstathiou & Rowan-Robinson (2003), the models of Bruzual & Charlot (1993, 2003) are used in combination with an assumed star formation history (SFH) to compute the spectrum of the starlight that is illuminating the dust throughout the model galaxy. Efstathiou & Rowan-Robinson (2003) assumed an exponentially decaying star formation rate $\dot{M}_*$, whereas here we assume a more general delayed exponential ($\dot{M}_* \propto t\, \mathrm{e}^{-t/\tau^s}$), where t is the time since the big bang and τ^s is the e-folding time of the exponential.

An important new feature of the spheroidal model is that the stars and dust are assumed to be mixed in a distribution that assumes a Sérsic profile with $n = 4$. A spherical geometry was chosen for the distribution of stars and dust, hence the name 'spheroidal'. The dust model used here is the same as that used in Efstathiou & Siebenmorgen (2009) and the models are computed with an adapted version of the spherically symmetric radiative transfer code used in the same work.

The spheroidal model assumes three parameters: the e-folding time of the delayed exponential τ^s, the optical depth of the spherical cloud from its centre to its surface τ_v^s, and the ratio of the central stellar emission to that of the intensity of starlight in the solar neighborhood ψ^s. The library used in this work was computed at a redshift of $z = 4.4$. We assumed that all the stars in the galaxy formed with a Salpeter initial mass function (IMF) from gas with a metallicity of 5 per cent solar, which appears to be typical of gas at such redshifts (e.g. Rafelski et al. 2012).

3.2 AGN torus and starburst models

We use the library of AGN torus models computed with the method of Efstathiou & Rowan-Robinson (1995) and described in more detail in Efstathiou et al. (2013). The method models the torus predicted by the AGN unified scheme with a smooth tapered disc distribution. The tapered disc consists of multiple species of dust of various sizes and compositions and its density declines as r^{-1}, where r is the distance from the central SMBH.

The AGN model parameters and their assumed range are the half-opening angle of the torus ($\Theta_0 = 30°$–$75°$), the inclination of the torus ($i = 0°$–$90°$), the ratio of inner to outer disc radius ($r_1/r_2 =$ 0.01–0.05) and the equatorial optical depth at 1000 Å ($\tau_{uv} = 250$–1250; in the dust model used in this work, this translates to $A_V \approx \tau_{uv}/5$ and $\tau_{9.7\mu\mathrm{m}} \approx \tau_{uv}/61$).

We use the starburst model originally developed by Efstathiou, Rowan-Robinson & Siebenmorgen (2000) and updated by Efstathiou & Siebenmorgen (2009). The model incorporates the stellar population synthesis model of Bruzual & Charlot (1993, 2003). The starburst model parameters and their assumed range are as follows: age of the starburst $t_* = 0$–30 Myr, GMC's(Giant Molecular Cloud) initial optical depth $\tau_V = 50$–250, and e-folding time of the exponentially decaying star formation rate (SFR) $\tau = 10$–30 Myr.

3.3 SED fitting and photo-*z* estimation with SATMC

We fitted the SED of HELP_J100156.75 + 022344.7 with the MCMC code SATMC (Johnson et al. 2013). SATMC can fit an SED given libraries of radiative transfer models and provides the option simultaneously to determine a photometric redshift that takes into account all the multiwavelength data used in the fit.

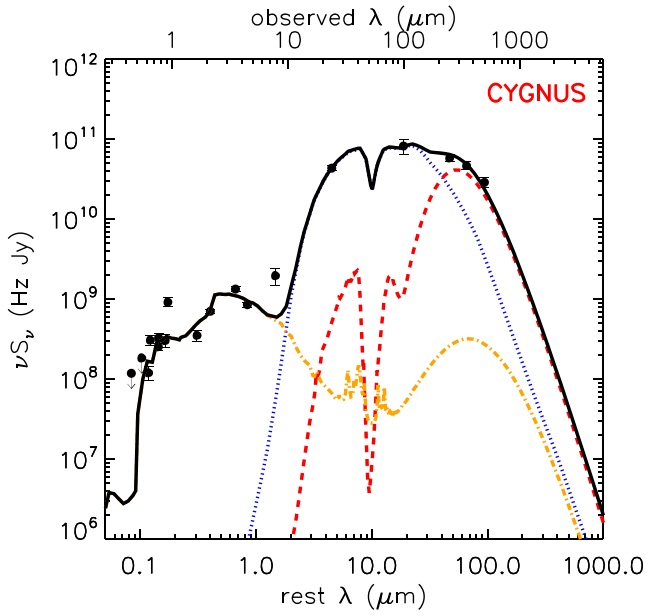

Figure 2. SED fit of HELP_J100156.75 + 022344.7 with CYGNUS models using libraries of starburst (red dashed), AGN torus (blue dotted), and spheroidal models (orange dot–dashed). The total emission is indicated by the solid black line.

SATMC predicts a photo-z of $4.71^{+0.76}_{-0.56}$ for HELP_J100156.75 + 022344.7, which agrees well with the photometric redshift estimates of 4.48 and 4.08 determined by Laigle et al. (2016) and Chang et al. (2017), respectively. We note that in the SUPRIME N921 filter we see an excess in the photometry that deviates significantly from the fit. If this is due to an emission line, it would need to be centred at around 1727 Å, assuming a redshift of 4.33, the value given in the HELP catalogue. The nearest strong quasar emission line is C III] with a rest wavelength of 1909 Å. If the excess is due to the C III] line, this would imply that the actual redshift of HELP_J100156.75 + 022344.7 is close to 3.82. Alternatively, there could be a problem with the SUPRIME N921 photometry.

In Fig. 2 we show the best fit of the SED obtained by fixing the redshift at 4.33. As the far-infrared and submillimetre photometry is very limited, we also fix the starburst age t_* at 10 Myr, the e-folding time of the starburst τ at 20 Myr, and ψ^s at 5. We have a total of 10 free parameters in the fit: τ^s, τ^s_v, Θ_0, i, r_1/r_2, τ_{uv}, τ_V, $f_{\rm AGN}$, f_s, and $f_{\rm SB}$. The last three are scaling factors that determine the luminosities of the AGN, spheroidal, and starburst components, respectively. The fit with SATMC is generally very good, apart from the discrepancies in the SUPRIME N921 filter and IRAC4. The discrepancy in IRAC4 may suggest the presence of polar dust (Efstathiou 2006; Efstathiou et al 2013).

SATMC determines and stores the best-fitting parameters of the models and their likelihoods. Each combination of model parameters stored by SATMC has been post-processed using our own routines to extract the physical quantities of HELP_J100156.75 + 022344.7 such as stellar mass, star formation rate, AGN fraction, and their uncertainties, and these are given in Table 2. We find, in particular, that HELP_J100156.75 + 022344.7 is an AGN-dominated object with 89 per cent of its 1–1000 μm luminosity of $3.91 \times 10^{13}\,{\rm L}_\odot$ provided by an obscured AGN. The covariances between the fitted parameters of both the photo-z fit and the fit with fixed z are plotted in Appendix B.

Table 2. Derived physical quantities and their 1σ uncertainties for HELP_J100156.75 + 022344.7 for the CYGNUS models and CIGALE. All listed luminosities are 1–1000 μm luminosities. The starburst SFR is averaged over 10 Myr in both CYGNUS and CIGALE. The minimum reduced χ^2 values of the best fits with CYGNUS and CIGALE are 4.3 and 4.8, respectively (see also Appendix A).

Quantity	CYGNUS	CIGALE	Unit
AGN luminosity	$3.47^{+1.79}_{-0.58}$	$1.27^{+0.07}_{-0.07}$	10^{13} L$_\odot$
Starburst luminosity	$4.34^{+1.12}_{-0.53}$	–	10^{12} L$_\odot$
Spheroidal luminosity	$9.54^{+3.27}_{-1.15}$	–	10^{10} L$_\odot$
Total luminosity	$3.91^{+1.69}_{-0.55}$	$1.72^{+0.06}_{-0.06}$	10^{13} L$_\odot$
Starburst SFR	1040^{+110}_{-269}	–	M$_\odot$ yr^{-1}
Spheroidal SFR	12^{+4}_{-2}	–	M$_\odot$ yr^{-1}
Total SFR	1051^{+109}_{-268}	991^{+223}_{-223}	M$_\odot$ yr^{-1}
Starburst stellar mass	$1.00^{+0.11}_{-0.26}$	–	10^{10} M$_\odot$
Spheroidal stellar mass	$4.03^{+1.04}_{-0.49}$	–	10^{10} M$_\odot$
Total stellar mass	$5.03^{+0.96}_{-0.45}$	$7.55^{+1.15}_{-1.15}$	10^{10} M$_\odot$
Core-collapse SN rate	$2.63^{+0.29}_{-0.68}$	–	SN yr^{-1}
AGN fraction	$0.89^{+0.05}_{-0.03}$	$0.74^{+0.04}_{-0.04}$	

4 DISCUSSION

In order to get an independent estimate of the main physical quantities we determined for HELP_J100156.75 + 022344.7 with CYGNUS, we also fitted the SED with the CIGALE code (Noll et al. 2009; Boquien et al. 2019). The main physical quantities extracted with CIGALE are tabulated in Table 2. This object was included in one of the HELP fields and was automatically fitted along with the other galaxies in the COSMOS field. The standard HELP fitting procedure, described in detail in Małek et al. (2018), estimated an AGN fraction of 80 ± 4 per cent. We performed dedicated SED fitting for this object using the CIGALE tool. We used the same modules as described in Małek et al. (2018), but, for the purposes of comparison in this work, we used a Salpeter IMF and a metallicity of 0.004 (2 per cent solar). For the HELP project in general, we used templates from the smooth models of Fritz et al. (2006) to model the AGN torus emission. Here we use the same module but with a denser grid of possible parameters of AGN fraction and angle between the equatorial axis and line of sight to constrain these parameters more accurately. The dedicated CIGALE fit shown in Fig. S1predicts an AGN fraction of 74 ± 4 per cent. The difference from the estimate from CYGNUS is most probably due to the ∼ 128 per cent anisotropy correction applied to the luminosity of the AGN torus of Efstathiou & Rowan-Robinson (1995); see also Efstathiou (2006). This correction is not applied in the AGN module in CIGALE. In any case, it should be noted that the agreement between the two results is remarkable, given the limited photometry and the significant differences in the methods used.

In Fig. 3 we compare the SED of HELP_J100156.75+022344.7 with that of the local deeply obscured ultraluminous infrared galaxy IRAS 08572 + 3915 (Efstathiou et al. 2014, $L \approx 10^{13}\,{\rm L}_\odot$), the $z = 2.74$ Hot DOG WISE 233759.50 + 792654.6 (Farrah et al. 2017, $L \approx 10^{14}\,{\rm L}_\odot$), and the $z = 4.05$ hyperluminous galaxy GN20 (Daddi et al. 2009, $L \approx 3 \times 10^{13}$ $_\odot$). According to the model of Efstathiou et al. (2014), IRAS 08572+3915 is a local AGN-dominated galaxy, which is estimated to have an AGN fraction of about 90 per cent. IRAS 08572+3915 is a much more obscured object compared with HELP_J100156.75 + 022344.7, with a very deep silicate absorption feature, as its torus is more optically thick. For

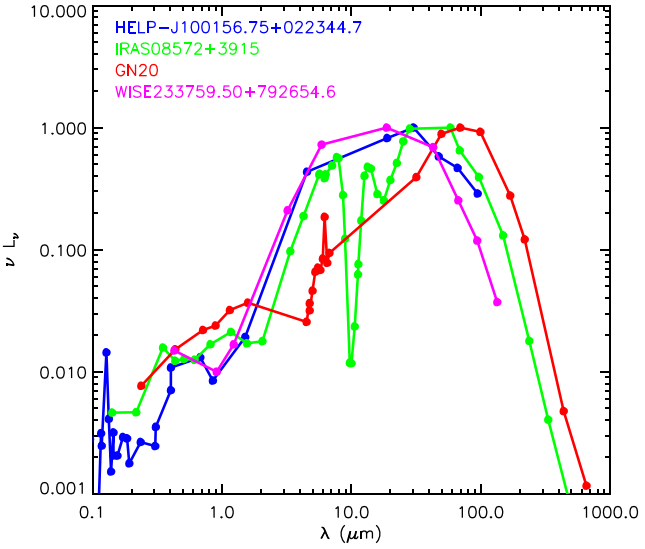

Figure 3. Comparison of the rest-frame SEDs of GN20 (red), IRAS 08572+3915 (green), WISE 233759.50+792654.6 (magenta), and HELP_J100156.75 + 022344.7 (blue). The SEDs have been normalized to their maximum νL_ν.

comparison, our CYGNUS fit predicts $\tau_{uv} = 261^{+66}_{-11}$ and $i = 88^{+0.9\circ}_{-0.7}$ for HELP_J100156.75+022344.7, whereas the corresponding values for IRAS 08572 + 3915 from the Efstathiou et al. (2014) fit were $\tau_{uv} = 500$ and $i = 88^\circ$. If there are objects similar to IRAS 08572 + 3915 at $z > 4$, they would generally be missed by current surveys such as *WISE* and HELP, because they are much fainter in the rest-frame mid-infrared. WISE 233759.50 + 792654.6, with a predicted AGN fraction of about 90 per cent (Farrah et al. 2017), has a very similar SED to HELP_J100156.75 + 022344.7.

The fact that the ultraviolet to far-infrared SED of HELP_J100156.75 + 022344.7 can be fitted very well with two independent methods and that the SED is similar to known lower redshift Hot DOGs gives us confidence that there is no contribution by a foreground galaxy in the spectrum. We therefore consider gravitational amplification unlikely.

As expected for an object that is dominated by star formation (Riechers et al. 2014), GN20 is fainter in the rest-frame mid-infrared compared with HELP_J100156.75 + 022344.7 by about an order of magnitude. Spinoglio et al. (2017) discussed the potential of a deep survey with the *Space Infrared Telescope for Cosmology and Astrophysics* (*SPICA*) at 34 μm to detect infrared galaxies up to redshift 6, assuming that such objects will have an SED similar to GN20. Fig. 3 suggests that objects like HELP_J100156.75+022344.7, IRAS 08572+3915, and WISE 233759.50 + 792654.6 will be much easier to detect and study with the *SPICA* and *James Webb Space Telescope* (*JWST*) spectrometers, compared with objects like GN20, if they exist at $z = 4$–6.

The space density of optically selected quasars at $z = 4$–5 with $M_{1450,AB} = -27$, which corresponds to a bolometric luminosity of a few times 10^{13} $L_\odot$, is about 10^{-8} Mpc^{-3} (Akiyama et al. 2018). We estimate the space density of objects like the one we have discovered as follows. The comoving volume between $z = 3$ and 6 for COSMOS, which we assume has an area of 1.7 deg^2, is 5.53×10^7 Mpc^3. This gives a space density of 1.8×10^{-8} Mpc^{-3}, which is slightly higher than the space density of optically selected quasars. This in turn implies that the covering factor of the obscuring torus in these objects is $\gtrsim 50$ per cent. This agrees well with the covering factor estimated from the Hot DOGs discovered by *WISE* (Assef et al. 2015) and the dust-reddened quasars in Faint Images of the Radio Sky at Twenty cm (FIRST) and the United Kingdom Infra-Red Telescope (UKIRT) Infrared Deep Sky Survey (UKIDDS: Glikman et al. 2013).

It is also interesting to compare the space density of obscured quasars at $z = 4$–6 with the observed space density of red sources in the redshift interval 4–6, which Duivenvoorden et al. (2018) estimate to be 1.1×10^{-8} Mpc^{-3}. Extreme starbursts and extreme AGNs are probably short-lived phenomena with similar duration, so estimates of their space density, once refined by analysing the complete HELP database, will give strong constraints on the coevolution of extreme AGNs and starbursts at those redshifts.

ACKNOWLEDGEMENTS

We thank an anonymous referee for useful comments and suggestions. HELP and the work leading to this article have received funding from the European Union Seventh Framework Programme FP7/2007-2013/ under grant agreement no. 607254. AE, DF, and VPL acknowledge support from the project EXCELLENCE/1216/0207/ GRATOS funded by the Cyprus RIF. KM has been supported by the National Science Centre (grant UMO-2018/30/E/ST9/00082).

DATA AVAILABILITY STATEMENT

The data underlying this article are available in the article.

REFERENCES

Akiyama M. et al., 2018, PASJ, 70S, 44A
Alexander D. M. et al., 1999, MNRAS, 310, 78
Antonucci R., 1993, ARA&A, 31, 473
Assef R. J. et al., 2015, ApJ, 804, 17
Banados E., 2018, Nature, 553, 473
Boquien M. et al., 2019, A&A, 622, 103
Bridge C. R. et al., 2013, ApJ, 769, 91
Bruzual A. G., Charlot S., 1993, ApJ, 405, 538
Bruzual A. G., Charlot S., 2003, MNRAS, 344, 1000
Cappelluti N. et al., 2009, A&A, 497, 635
Chang Y. et al., 2017, ApJS, 33, 19
Daddi E. et al., 2009, ApJ, 694, 1517
Delvecchio I. et al., 2014, MNRAS, 439, 2736
Diaz-Santos T. et al., 2018, Science, 362, 1034
Duivenvoorden S. et al., 2018, MNRAS, 477, 1099
Efstathiou A. et al., 2013, MNRAS, 436, 1873
Efstathiou A. et al., 2014, MNRAS, 437, L16
Efstathiou A., 2006, MNRAS, 371, L70
Efstathiou A., Rowan-Robinson M., 2003, MNRAS, 343, 322
Efstathiou A., Rowan-Robinson M., 1995, MNRAS, 273, 649
Efstathiou A., Rowan-Robinson M., Siebenmorgen R., 2000, MNRAS, 313, 734
Efstathiou A., Siebenmorgen R., 2009, A&A, 502, 541
Eisenhardt P. R. M. et al., 2012, ApJ, 755, 173
Fabian A. C., 2012, ARA&A, 50, 455
Farrah D. et al., 2002, MNRAS, 335, 1163
Farrah D. et al., 2003, MNRAS, 343, 585
Farrah D. et al., 2012, ApJ, 745, 178
Farrah D. et al., 2017, ApJ, 844, 106
Frayer D. T. et al., 2009, AJ, 138, 1261
Fritz J. et al., 2006, MNRAS, 366, 767
Glikman E. et al., 2013, ApJ, 778, 117
Harris K. et al., 2016, MNRAS, 457, 4179
Herrero-Illana R. et al., 2017, MNRAS, 471, 1634
Hickox R. C., Alexander D.M., 2018, ARA&A, 52, 625

Hurley P. D. et al., 2017, MNRAS, 464, 885
Johnson S. P. et al., 2013, MNRAS, 436, 2535
Jones S. F. et al., 2015, MNRAS, 448, 3325
Kelly B. C. et al., 2010, ApJ, 719, 1315
Laigle C. et al., 2016, ApJS, 224, 24
Lonsdale C. J. et al., 2015, ApJ, 813, 45
Małek K. et al., 2018, A&A, 620, 50
Marchesi S. et al., 2016, ApJ, 817, 34
Mattila S. et al., 2012, ApJ, 756, 111
Mattila S. et al., 2018, Science, 361, 482
Mortlock D. J. et al., 2011, Nature, 474, 616
Noll S. et al., 2009, A&A, 507, 1793
Pilbratt G. L. et al., 2010, A&A, 518, 1
Pitchford K. et al., 2019, MNRAS, 487, 3130
Rafelski M. et al., 2012, ApJ, 755, 89
Riechers D. A. et al., 2014, ApJ, 786, 31
Ruiz M. et al., 2001, MNRAS, 325, 995
Scoville N. et al., 2007, ApJS, 172, 1
Shirley R. et al., 2019, MNRAS, 490, 634
Smolcic V. et al., 2017, A&A, 602, 1
Spinoglio L. et al., 2017, PASA, 34, 57
Tsai C.-W. et al., 2015, ApJ, 805, 90
Tsai C.-W. et al., 2018, ApJ, 868, 15
Verma A. et al., 2002, MNRAS, 335, 574
Vito F. et al., 2018, MNRAS, 473, 2378
Wang F., 2018, ApJ, 869, L9
Wu X.-B. et al., 2015, Nature, 518, 512
Yang J. et al., 2020, ApJL, 897, L14

SUPPORTING INFORMATION

Supplementary data are available at *MNRASL* online.

Figure S1 Best fit to the SED of HELP_J100156.75 + 022344.7 with CIGALE.

Figure S2 Plot showing the covariances between the parameters of the SED fit of HELP_J100156.75 + 022344.7 with the CYGNUS models and using the photo-z option of SATMC.

Figure S3 Same plot as Fig, S2, showing the covariances between the parameters of the SED fit of HELP_J100156.75 + 022344.7 with the CYGNUS models and z fixed at 4.33.

Figure S4 Plot showing the p-value maps at 250, 350 and 500 μm.

Please note: Oxford University Press is not responsible for the content or functionality of any supporting materials supplied by the authors. Any queries (other than missing material) should be directed to the corresponding author for the article.

This paper has been typeset from a TEX/LATEX file prepared by the author.